IEEE Access
Multidisciplinary | Rapid Review | Open Access Journal

Received February 2, 2020, accepted March 29, 2020, date of publication April 8, 2020, date of current version March 26, 2021.

Digital Object Identifier 10.1109/ACCESS.2020.2986481

A Torque Control Method Based on *I-MR* Controller for IPMSM Drive With Small DC-Link Capacitor

HAICHUN LI[1], QUAN YIN[1], QINGYI WANG[2], JIGUI MIAO[1], AND YANTING HOU[3]
[1]School of Artificial Intelligence and Automation, Huazhong University of Science and Technology, Wuhan 430000, China
[2]School of Automation, China University of Geosciences, Wuhan 430000, China
[3]Guangdong Elesy Electric Company, Ltd., Foshan 528305, China

Corresponding author: Quan Yin (yinquans_hust@163.com)

This work was supported in part by the National Natural Science Foundation of China under Grant 61374049.

ABSTRACT In traditional motor drive system, large volume electrolytic capacitors are utilized to buffer energy and stabilize the dc-link voltage. However, these capacitors affect the reliability of the drives and narrow the conduction angle of diode-rectifier. As a result, the grid side current is distorted and the power factor is deteriorated. In order to settle these issues, small dc-link capacitors can replace the electrolytic capacitors. In this paper, a motor torque control method with dc-link voltage feed-forward compensation for an interior permanent magnet synchronous motor (IPMSM) drive system is proposed. Hence, an integration multi-resonant (*I-MR*) controller is established to regulate the motor torque to obtain high input power factor and low grid current harmonics. In addition, a voltage feed-forward compensation is used to diminish the error of motor torque control. The effectiveness of the proposed method is verified through simulation and experiments. Results indicate that the input power factor can reach about 99.4% and the grid current harmonics are considerably lower than the requirement of EN-61000-3-2 standard.

INDEX TERMS IPMSM, small dc-link capacitor, high power factor, torque control, integration multi-resonant controller, voltage feed-forward compensation.

I. INTRODUCTION

Nowadays, interior permanent magnet synchronous motors (IPMSMs) have been widely used in industrial and white home applications due to their superior efficiency, power density and torque-to-inertia ratio [1]–[3]. Generally, in traditional AC-DC-AC IPMSM drive systems, large capacity electrolytic capacitors are utilized at dc-link to buffer energy and stabilize the voltage. It may lead to high cost, large volume, short lifetime and greatly affect the competitiveness of the system in the industrial applications [4]–[7]. Furthermore, the single-phase diode-rectifier has narrow conduction angle and the input current is pulsating. This discontinuous current contains many high order harmonics, which lead to distortion of input current and deterioration of grid power factor. Thus, the grid input performance for the IPMSM drive system is degraded [8].

In order to solve these problems, the small dc-link capacitor IPMSM drive system has been developed. A film or ceramic capacitor can replace the electrolytic capacitor, as shown in Fig. 1. This topology consists of a single-phase diode-rectifier, a film capacitor and three-phase voltage-source inverter. Compared to electrolytic capacitor, the film capacitor has high reliability and less capacitance per unit [9], [10], which can reduce the overall system volume and cost. Meanwhile, with capacitance at dc link remarkably decreased, there is no device to store energy, the current can be flowed into the inverter directly. Thus, the input current becomes smoothly, and the grid quality of the system can be improved.

To obtain a high power factor and low grid harmonics in small dc-link capacitor drive system, many research efforts have gone into the development of power factor control. Many power factor correction (PFC) topologies [11]–[15], such as DC-link shunt compensator (DSC) have been recently employed in [11]–[13]. However, the PFC circuits must have additional isolation, electrolytic capacitors and switching devices. It increases the cost and the volume and is not suitable for the economical motor drive system.

The associate editor coordinating the review of this manuscript and approving it for publication was Ton Do.

In addition to the topology modification, an inverter power control method was proposed in [9], [10], [16]–[20]. The power control loop was cascaded between the speed loop and current loop based on the relationship between gird side input and inverter output power. Then, a lot of power controllers were implemented to control grid power factor and the input current harmonics. A proportional-integrational (PI) controller was applied in [16], however, the power factor is satisfied only at rated load. In [17], the repetitive controller was proposed to replace the PI controller. It has the ability to learn signal model and achieve better control performance when tracking periodic signals. But the digital implementation is complicated. A proportional-resonant (PR) controller [18] and a proportional-integrational-resonant (PIR) [19] controller were proposed. The resonant (R) controller can track sinusoidal signal at grid input frequency better. Son et al proposed a direct power control method in [20]. It computes *d-q* axis current reference offline at several operating points, but the robustness of the proposed method is weak and load condition is necessary for offline calculation. Therefore, the gain of all these power controllers cannot be designed because of the nonlinearity caused by the inverter output power feedback.

Hence, to improve the drawbacks of power control method, the motor torque control strategy was proposed in [21]–[23]. As the speed is approximate considered to a constant value, the power control strategy can be converted into a linearization control system. Thus, comparing to the power control method, the motor torque control focuses on the relationship between the input power and the motor torque. It replaced the power control to generate the q-axis current reference. In this torque control system, the integration resonant (IR) [21], [22] and integration quasi-resonant (IQR) [23] controller were proposed, which consists of an integrator and a sinusoidal tracking controller. It is easy to design the controller parameters to achieve a high power factor by the linearization of the control system. But these control methods only focused on the input current fundamental components.

In order to obtain high grid power factor and suppress the input current harmonics for small capacitor IPMSM drive system, this paper proposes a motor torque control method including torque control loop based on integration multi-resonant (*I-MR*) controller and voltage feed -forward compensation strategy. The motor torque control loop is established to regulate the motor torque to track the input power, which guarantees the grid input current to be sinusoidal signals. Then, the *I-MR* controller is designed to calculate q-axis current reference, comparing to the power control system, the gain of the controller is easy to design under the torque transfer function and simple control structure, so the physical meaning is clearly. Moreover, with the limitation of current control bandwidth and the dc-link voltage insufficient, the motor torque can't follow the reference well. The voltage feed-forward compensation strategy is applied to reduce torque control error, which improves the torque control performance. Therefore, the grid input current harmonics are suppressed, and the quality of the input current can be improved.

This paper is organized as follows. Section II analyzes the torque characteristics of the small dc-link capacitor drive system, and the principle of motor torque control is presented. In Section III, the proposed motor torque control method based on *I-MR* controller is discussed and realized, including the controller parameters designing and stability analysis. The voltage feed-forward compensation is presented in Section IV. Finally, the effectiveness of the proposed control method is verified by simulations and experiments.

II. PRINCIPLE OF MOTOR TORQUE CONTROL

As the large-capacity electrolytic capacitor is replaced by the small film capacitor, there is no energy buffer at dc-link. The IPMSM drive system not only controls the motor but also the grid power factor [21]. Therefore, the relationship between the power factor and the motor torque control is described below.

In order to obtain high power factor and reduce grid current harmonics, the grid input current must be synchronized with grid voltage. The grid voltage u_g, grid current i_g and the expected grid power P_g can be presented as follows:

$$\begin{aligned} u_g &= U_g \sin(\theta_g) \\ i_g &= I_g \sin(\theta_g) \\ p_g &= u_g i_g = U_g I_g \sin^2(\theta_g) \end{aligned} \tag{1}$$

where U_g and I_g are grid input voltage amplitude, current amplitude, respectively. θ_g is the phase angle of the grid.

Ignoring the line resistance, inductance and the voltage drop on diode rectifier, the dc-link voltage is approximate to the absolute value of the grid source voltage due to the low capacitance of film capacitor. It cannot maintain a constant value and fluctuate with twice the frequency of grid voltage, so the dc-link voltage and capacitor power p_c can be calculated as follows:

$$\begin{aligned} u_{dc} &= \left|U_g \sin(\theta_g)\right| \\ p_c &= C_{dc} u_{dc} \frac{du_{dc}}{dt} = \frac{1}{2}\omega_g C_{dc} U_g^2 \sin(2\theta_g) \end{aligned} \tag{2}$$

where ω_g is angular speed of the AC grid, C_{dc} is the capacitance of the dc-link capacitor.

According to Fig. 1, the inverter output power p_{inv} can be obtained by subtracting the capacitor power p_c from the grid input power p_g. It can be calculated as follows:

$$p_{inv} = p_g - p_c \tag{3}$$

By substituting Eq. (1) and Eq. (2) into Eq. (3), the inverter output power p_{inv} is obtained:

$$\begin{aligned} p_{inv} &= U_g I_g \sin^2(\theta_g) - \frac{1}{2}\omega_g C_{dc} U_g^2 \sin(2\theta_g) \\ &= \frac{1}{2} U_g I_g - \frac{1}{2} U_g I_g \sqrt{1 + (\frac{Y_c}{Y_g})^2} \sin(2\theta_g + \phi) \\ &= \bar{P}_{inv} + \tilde{P}_{inv} \sin(2\theta_g + \phi) \end{aligned} \tag{4}$$

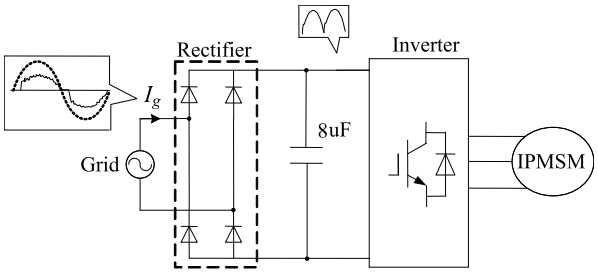

FIGURE 1. Circuit diagram of the inverter with small dc-link capacitor.

where $\bar{P}_{inv}$ is the dc component, $\tilde{P}_{inv}$ is the ac component. Y_c, Y_g are the dc-link capacitor and grid input equivalent admittance, respectively. ϕ is the power phase.

Considering the motor voltage equation in the d-q reference frame, and the electrical losses other than the copper loss as p_{loss}, the inverter output power p_{inv} is represented as:

$$\begin{aligned} p_{inv} &= \frac{3}{2}(u_d i_d + u_q i_q) \\ &= \underbrace{1.5\omega_{rm} i_q[\varphi_f + (L_d - L_q) i_d]}_{p_m} \\ &\quad + \underbrace{1.5(L_d i_d \frac{di_d}{dt} + L_q i_q \frac{di_q}{dt})}_{p_{mag}} + \underbrace{1.5R_s(i_d^2 + i_q^2)}_{p_{loss}} \end{aligned} \quad (5)$$

where i_d, i_q, L_d, L_q, R_s, φ_f and ω_r are the dq-axis currents, the dq-axis inductors, the stator resistor, the permanent flux of the motor and motor mechanical angular speed, respectively. p_m is the motor mechanical power, p_{mag} is the inductive power by change of the current and p_{loss} is the copper loss.

In addition, for the motor mechanical time constant is much larger than the electromagnetic time constant, the motor speed ω_r is approximate considered to a constant in one switch cycle. Converting power dimension into equivalent torque, the grid input equivalent torque τ_s is obtained:

$$\begin{aligned} \tau_s &= \frac{p_g}{\omega_r} = \frac{p_c}{\omega_r} + \frac{p_m}{\omega_r} + \frac{p_{mag}}{\omega_r} + \frac{p_{loss}}{\omega_r} \\ &= \tau_c + \tau + \tau_{mag} + \tau_{loss} \\ &= \tau_c + \tau_{inv} \end{aligned} \quad (6)$$

where τ_c is capacitor equivalent torque, τ is the motor mechanical torque, τ_{mag} is the inductive equivalent torque, τ_{loss} is the copper loss equivalent torque and τ_{inv} is the inverter output equivalent torque.

When the dc-link capacitance is very small, it is obviously that $\tau_c \ll \tau_{inv}$. The sharp of the grid input current can be directly affected by the output equivalent torque of the inverter. A high power factor can be obtained by controlling the inverter output torque on the basis of Eq. (6).

Based on the torque analysis above, in order to achieve high power factor and low THD of the grid current, the purpose of torque control method is to ensure the grid input equivalent torque to be sinusoidal. According to Eq. (6), the grid input torque consists of the film capacitor torque and the inverter torque. The inverter torque can be calculated according to Eq. (5). When the input source voltage and frequency is set, the film capacitor equivalent torque only determined by the capacitance at dc-link, and it is much smaller than the inverter torque. As a result, the inverter output torque should track the expected grid equivalent torque effectively.

III. THE MOTOR TORQUE CONTROL METHOD

Fig. 2 shows the block diagram of the proposed motor control method. The system consists of a speed control loop, motor torque control loop and current control loop. The motor torque *I-MR* controller is cascaded between speed and current controllers, which generates the q-axis current reference. It is possible to regulate the inverter output torque to track the grid input torque. And make the diode rectifier current continuous to reduce the grid current harmonics. Meanwhile, a voltage feed-forward compensation is adopted to diminish the torque control error. It modifies the inverter voltage vector to improve the torque control performance. Furthermore, to ensure the high speed of the motor and the input power factor [16] during low dc-link voltage range, the d-axis current generator is used for flux-weakening control. The detailed analysis of the proposed control methods are illustrated as follows.

Fig. 3 shows the block diagram of the inverter motor torque loop. According to Eq. (6), the output of the speed controller T_e^* is the average equivalent torque produced by the grid input power. The grid input equivalent torque reference τ_s^* is obtained by multiplying T_e^* and $sin^2(\theta_g)$. Here, the θ_g is detected from a phase locked loop in [24]. The inverter output torque reference τ_{inv}^* is obtained by subtracting τ_c from τ_s^*. If the inverter output torque can be regulated precisely, a unity power factor is obtained [23].

Actually, the motor torque controller controls the motor torque and the grid input current. It improves the grid input performance by controlling the motor torque. According to Eq. (3) and Eq. (6), the inverter torque τ_{inv} can be represented as:

$$\tau_{inv} = \bar{\tau}_{inv} + \tilde{\tau}_{inv} \sin(2\theta_g + \phi) \quad (7)$$

It can be seen that inverter torque τ_{inv} consists of two components. The first item is the dc component, and the second item is ac component, which is a periodic sinusoidal signal with twice frequency of grid source voltage. To achieve unit power factor, the output torque of the inverter needs to be preciously controlled to track the sinusoidal input torque. Therefore, a suitable controller should be designed for a small capacitor drive system.

Based on the internal model principle, the resonant (R) controller can be used to track alternating signals without any steady-state errors. So the integration resonant (IR) controller can be adopted to replace the PI type controller and eliminate the tracking error. An integrator $1/s$ and resonant controller $s/(s^2 + \omega 20)$ in [25], [26] that targets at twice frequency of AC source voltage should be contained in the motor torque controller. The transfer function of ideal

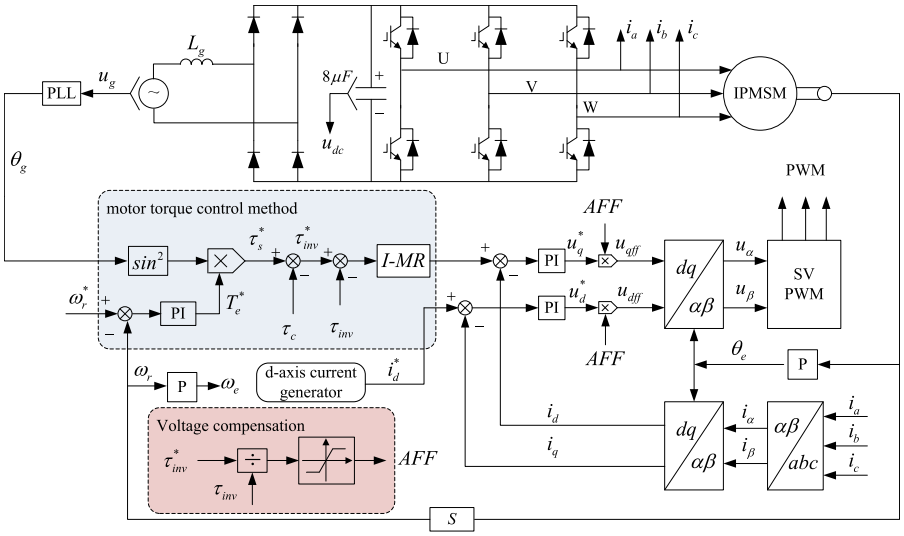

FIGURE 2. Control block diagram of motor torque method with small dc-link capacitor.

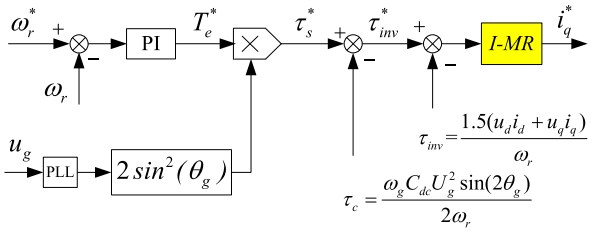

FIGURE 3. Diagram of the inverter with small dc-link capacitor.

resonant controller can be expressed as

$$G_R(s) = \frac{K_r s}{s^2 + \omega_0^2} \tag{8}$$

where K_r is resonant gain, ω_0 is resonant frequency. Since only alternate components compose the inverter current references, the conventional ideal resonant controller does not guarantee zero error in steady state. Thus, the integral-multi resonant (*I-MR*) controller is adopted [27]–[29]. The transfer function of *I-MR* controller $G_{I-MR}(s)$ is given as

$$G_{I-MR}(s) = \frac{K_i}{s} + \sum_{n=1}^{M} \frac{K_{rn} s}{s^2 + (n\omega_0)^2} \tag{9}$$

where K_i is the integral gain, K_{rn} is resonant gain at a specific resonant frequency, $n = 1, 3, 5, 9, \ldots,$ M, which represent the first, third, fifth, seventh, and ninth input current components.

Fig. 4 shows the bode diagram of the multi resonant (*MR*) controller with $n = 1, 3$ at different gains such as $Kr1, 3 = 10, 60$, and 200, respectively. It can be concluded that K_{rn} affects the gain of the controller. When the K_{rn} increases, the gain at resonant frequency increases too.

Based on the above analysis of the *I-MR* controller characteristics, the AC component can be control by

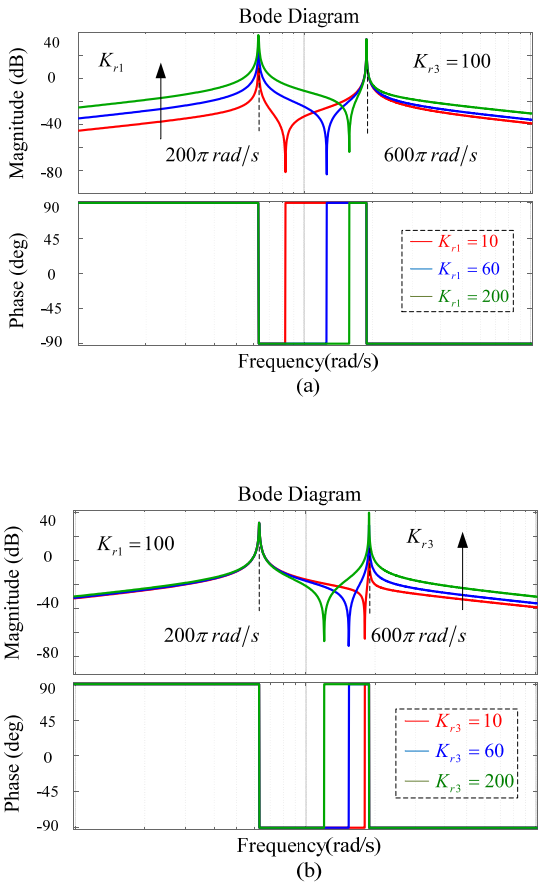

FIGURE 4. Bode diagram of multi resonant controller. (a) K_{r1}. (b) K_{r3}.

parameter K_{rn}, while the DC component can be control by parameter K_i. In small capacitor drive systems, considering the sampling delay and the pulse width modulation (PWM) delay time, it assumes that the motor current can track the

reference with no state error which means $i_q^* \approx i_q$. The motor torque control loop with *I-MR* controller can be setup as shown in Fig. 5.

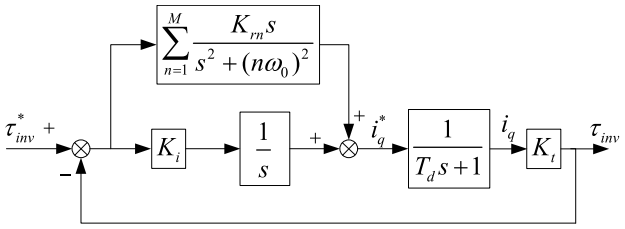

FIGURE 5. Block diagram of motor torque control loop.

where T_d is the time delay of current control loop, K_t is torque coefficient. According to Fig. 5, there are two important control parameters, the first is K_i. When $K_{rn} = 0$, the DC component $\bar{\tau}_{inv}$ passes through integration controller by neglecting the AC component $\tilde{\tau}_{inv}$. The closed loop transfer function can be simplified as a typical second order model as follows:

$$G_{dc}(s) = \frac{\bar{\tau}_{inv}}{\bar{\tau}_{inv}^*} = \frac{K_i K_t}{s(T_d s + 1) + K_i K_t} = \frac{\omega_t^2}{s^2 + 2\varepsilon\omega_t s + \omega_t^2} \tag{10}$$

where ω_t is the natural frequency of the system, ε is the damping coefficient. Then the integration gain K_i can be set as:

$$K_i = \frac{\omega_t}{2\varepsilon K_t} \tag{11}$$

The other parameter is K_{rn}. When $K_i = 0$, the equivalent open-loop transfer function with respect to the resonant gain K_{rn} is given by

$$H_r(s) = \frac{K_t K_{rn} s}{(T_d s + 1)(s^2 + (n\omega_0)^2)} = \frac{K_a s}{(s + \tau_d)(s^2 + (n\omega_0)^2)} \tag{12}$$

where $K_a = K_t K_{rn} \tau_d$ is the equivalent open-loop gain, $\tau_d = 1/T_d$. In order to analyze the system stability and turn the controller parameters, the sampling time was set to $50\mu s$, and Eq.(12) was transfered into discrete time domain. The root locus of the close-loop with K_a changes from 0 to infinite is shown in Fig. 6. Obviously, while the resonant frequency $n\omega_0$ changes, the closed-loop characteristic roots can be located inside the unit circle boundary in the z plane, which indicates a stable system.

In Fig. 6, the closed-loop characteristic roots move toward to the outside of the unit circle, and the stability margin weakens while K_{rn} increases. Then, the resonant gain K_{rn} should be selected as $K_{rn} < 193$. In addition, the damping ratio is usually selected around 0.707, and the overshoot of the motor torque is configured below 10%. Then, parameters of the *I-MR* controller is selected as $K_{r1} = 30$ in this case to achieve sufficient stability margin as well as relatively high gain around the resonant frequency.

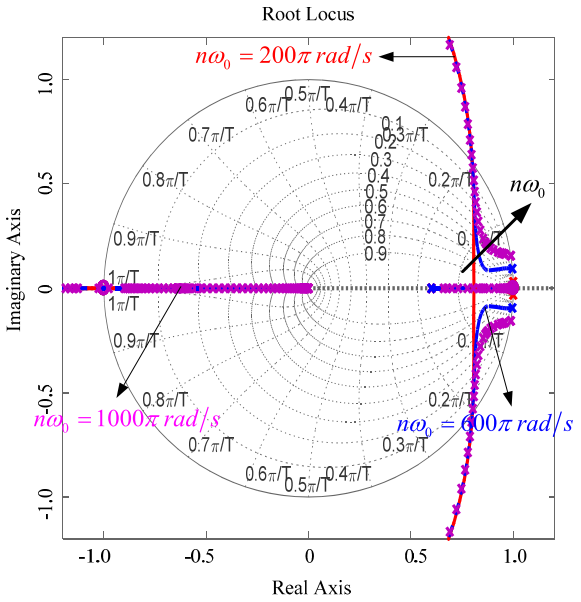

FIGURE 6. Root locus of the I-MR controller.

On the basis of analysis above, it can be found that the proposed motor torque controller has low magnitude attenuation and phase delay at resonant frequency point. It can achieve rapid response to ensure dynamic performance of motor drive system.

IV. VOLTAGE FEED-FORWARD COMPENSATION

The motor torque controller regulates the inverter output torque to track the grid input torque well. But in small capacitor drive system, with limitation of the current control loop, the error between the torque reference τ_{inv}^* and the actual feedback torque τ_{inv} can't be completely eliminated only by adopting the *I-MR* controller. It is difficult to achieve the ideal control effect.

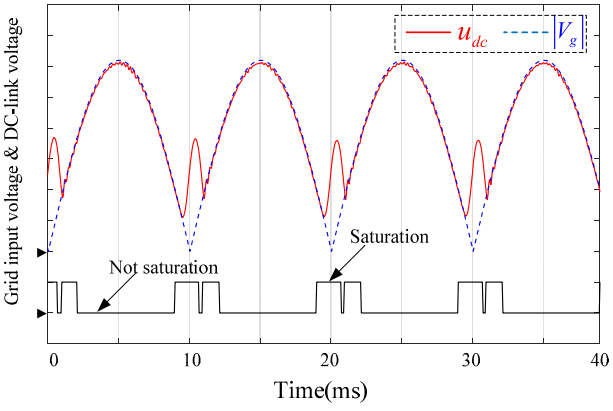

FIGURE 7. Simulation results of the dc-link voltage and voltage saturation state.

In addition, without large electrolytic capacitors at dc-link, the dc-link voltage fluctuates with twice the frequency of grid source voltage. During the voltage valley, as shown in Fig. 7,

the current controller and the PWM will saturate that the motor current can't follow the reference, and motor current would flow into dc-link capacitor at high speed. Then, the grid input current will be clamped when crossing zero. As a result, the conduction angle of diode-rectifier is narrowed and the input power factor is reduced.

In order to solve above problems, a voltage feed-forward compensation is applied to improve torque control performance. The inverter output voltage modification strategy is described as below:

$$AFF = \frac{\tau^*_{inv}}{\tau_{inv}} \tag{13}$$

$$\begin{cases} u_{dff} = AFF \cdot u^*_d \\ u_{qff} = AFF \cdot u^*_q \end{cases} \tag{14}$$

where AFF is the voltage correction coefficient, u^*_d and u^*_q are the outputs of the current controller, the u_{dff} and u_{qff} are the voltage vector references of the inverter.

According to Eq.(13) and Eq.(14), when $\tau^*_{inv} \approx \tau_{inv}$, the motor torque can track the reference well and AFF = 1, that means the voltage does not need to be modified. But when $\tau^*_{inv} \neq \tau_{inv}$, especially the voltage is insufficient, the voltage correction starts automatically. For the tracking performance of the d-q currents is limited by the bandwidth of the current control loop, the controller outputs would delay after the actual voltage. The voltage feed-forward can correct the inverter output voltage in real time, which improves the inverter torque response to compensate the deficiency of the current control bandwidth.

The AFF must be limited to avoid abrupt changes in the output voltage, which would destroy the inverter and degrade grid performance.

V. SIMULATION RESULTS

In order to verify the validity of the torque control method, the proposed system from Fig. 2 has been implemented in the Matlab/Simulink programming environment. The simulation parameters are listed in Table 1.

TABLE 1. Drive and system parameters.

PARAMETERS	Value	PARAMETERS	Value
Rate power	1.0 kW	Flux linkage	0.104 Wb
Maximum speed	3900 r/min	Switching frequency	10 kHz
Rate speed	2000 r/min	Film capacitor	8 uF
Pole pairs	4	Grid voltage	220 V
d-axis inductance	4.94 mH	Grid frequency	50 Hz
q-axis inductance	10.74 mH	Line resistance	0.5 Ω
Stator resistance	0.845 Ω	Line inductance	0.2 mH

In the system, the dc-link capacitor C_{dc} is only 8 μF, the speed and current controller adopt PI regulator, and the bandwidth would be set lower than electronic capacitor drives to ensure the stability of the system. The dc-link voltage drops near zero periodically, as shown in Fig. 7, so the average value of the dc-link voltage is lower than conventional one with large electrolytic capacitors. Flux weakening method like [16], [30], [31] should be applied to control the d-axis current. However, the most well-known d-axis current control method is not suitable for reduced dc-link capacitance IPMSM drive system. In this paper, average voltage constraint in [16] is applied for such system to obtain a high power factor. Since the maximum speed of motor is about 3900 r/min, all of these simulations and experiments were at 3.2Nm, 2000r/min. The detailed analysis of the results is illustrated as follows.

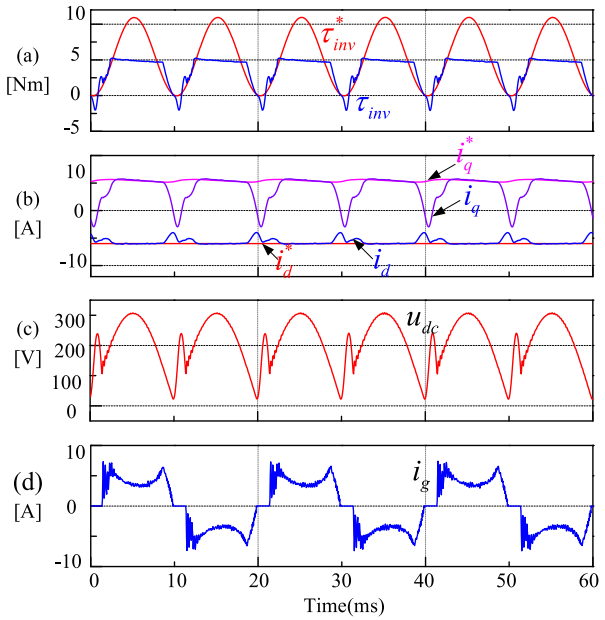

FIGURE 8. Simulation results of small capacitor drive system without any proposed control scheme. (a) The motor torque and reference; (b) the dq-axis current and references; (c) dc-link voltage; (d) grid input current.

Fig. 8 shows the simulation results of small capacitor drive system without any proposed control method. In Fig. 8(a) and Fig. 8(b), the motor torque and dq-axis current can't track its references. Meanwhile, the input current distorts severely. As a result, the harmonics of grid current far exceed the standards of EN-61000-3-2.

Fig. 9 shows the simulation results of the proposed motor torque control method with M = 1. Obviously, the motor torque and dq-axis current can track its references better. At the same time, the grid input current approximates the sinusoidal signal, and the power factor and THD of the grid side are 0.994 and 10.59%. Nevertheless, in the input current waveform, there are many high order frequency oscillations especially when crossing zero.

Fig. 10 shows the simulation results of torque control method with M = 5, the *I-MR* controller is applied. Compared to Fig. 9, the amplitude of high frequency oscillations decreased, and the input current waveform becomes more smoothly. Therefore, the high order harmonics is also reduced.

Fig. 11 shows the simulation results of torque control loop with voltage compensation strategy. It can be seen that the

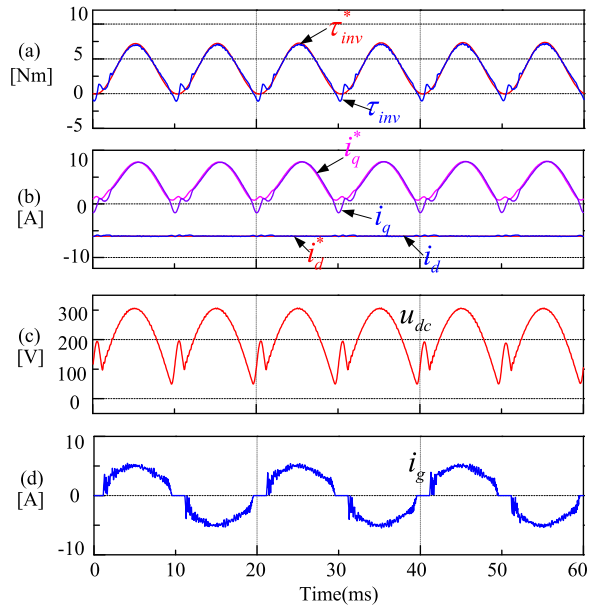

FIGURE 9. Results of torque control method with M = 1. (a) The motor torque and reference; (b) the dq-axis current and references; (c) dc-link voltage; (d) grid input current.

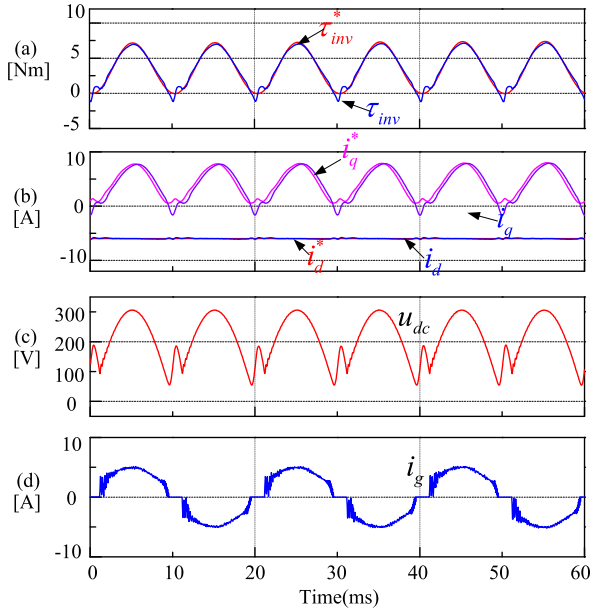

FIGURE 10. Results of torque control method with M = 5. (a) The motor torque and reference; (b) the dq-axis current and references; (c) dc-link voltage; (d) grid input current.

motor torque response and the input current response are improved. The input current harmonics are uniformly distributed and effectively suppressed.

Fig. 12 shows FFT analysis results of the proposed torque control with voltage compensation method in simulation. However, under this ideal conditions, the motor load, current, torque and power are very smooth. Moreover, the sampling delay and the digital control delay are not considered. So the

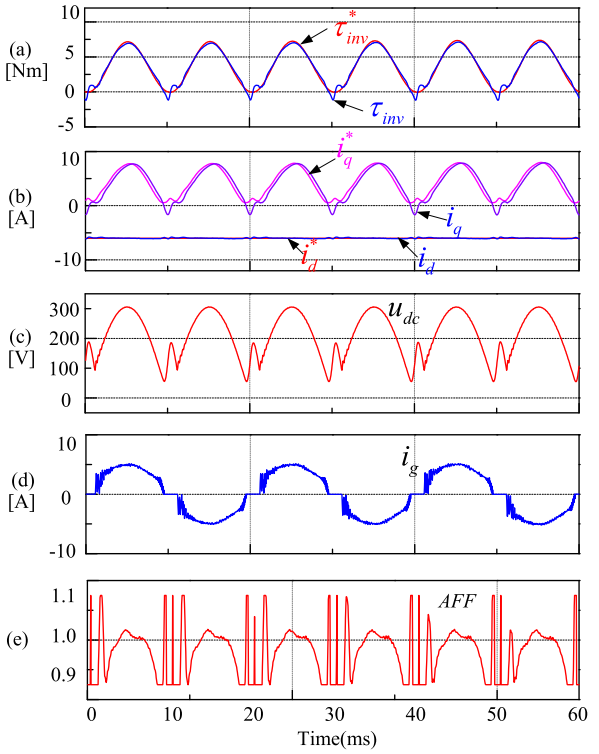

FIGURE 11. Results of torque control method with voltage compensation. (a) The motor torque and reference; (b) the dq-axis current and references; (c) dc-link voltage; (d) grid input current; (e) voltage compensation gain AFF.

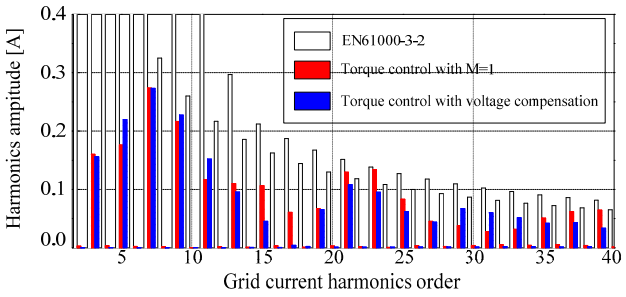

FIGURE 12. FFT analysis result of grid input current in simulation.

voltage feed-forward control is not very obvious. But the grid input current still meets the standards of EN-61000-3-2.

VI. EXPERIMENTAL RESULTS

To further verify the performance of the proposed control methods, the motor torque control platform of IPMSM based on *I-MR* controller was constructed. Experimental hardware is shown in Fig. 13. In Fig. 13(a) and Fig. 13(b), the load motor is used as generator and consumes power at a load resistor. The inverter is realized by Mitsubishi module PS21767. The grid input voltage and frequency are 220Vrms and 50 Hz. The proposed control methods were implemented with a Texas Instruments TMS320F28075 floating-point digital signal processor. The parameters of the experiment are the same as the simulation, as indicated in Table 1.

(a)

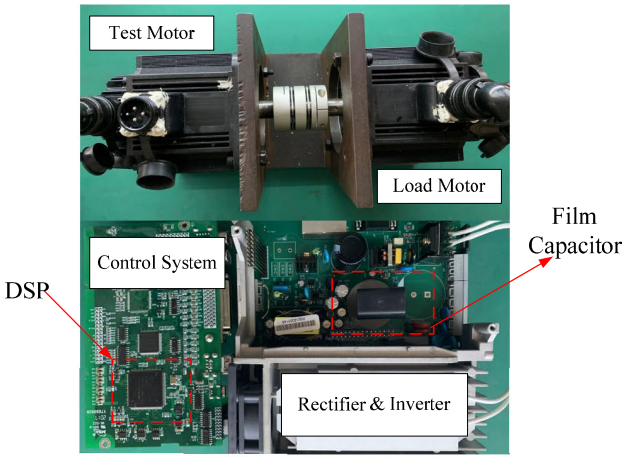

(b)

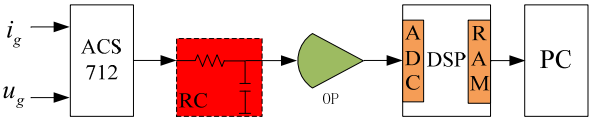

(c)

FIGURE 13. Experiment hardware configuration. (a) Overall diagram of the hardware; (b) the small capacitor drive configuration; (c) experimental data sampling circuit.

Fig. 13(c) shows grid input voltage and current sample circuits, all of experimental data is read in this way. Therefore, the hall sensor and Low pass filter (*RC*) would filter out a lot of higher order harmonics such as the switching noise of IGBT, but the distribution of the harmonics complies with simulation result.

In this paper, the average voltage constraint in [16] is applied for such system to obtain a high power factor. The average DC-link voltage can be calculated as fallow [4]:

$$U_{av} = \frac{1}{\pi}\int_0^{\pi} U_g \sin(\theta_g) d\theta_g = \frac{2}{\pi} U_g = 197V \qquad (15)$$

Since the maximum speed of motor is about 3900r/min, the maximum average speed is about $3900^*2/\pi = 2500$r/min.

Similarly, according to Eq. (7), the ideal output torque of the motor can be obtained by:

$$\tau_{inv} \approx 3.2 + 3.2\sin(2\theta_g + \phi) \qquad (16)$$

Thus, the average torque is 3.2Nm, and the peak value is about 6.4Nm.

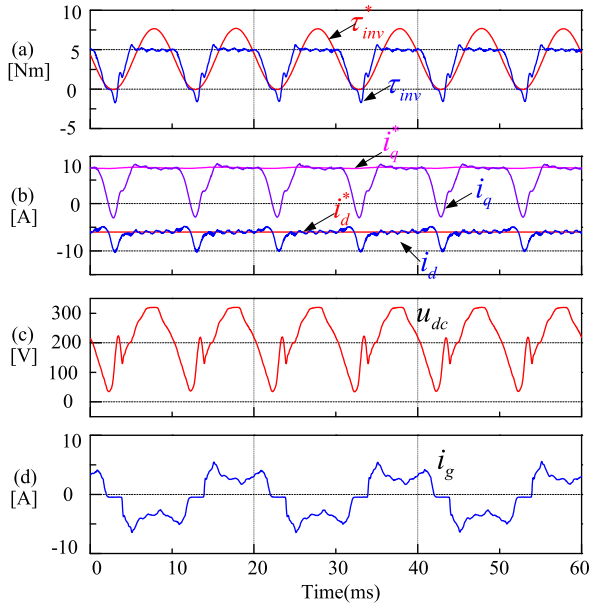

FIGURE 14. Results of small capacitor drive system without any proposed control scheme. (a) The motor torque and reference; (b) the dq-axis current and references; (c) dc-link voltage; (d) grid input current.

Fig. 14 shows the experiment results of small capacitor drive system without any proposed control method. From both the simulation and experimental results, it shows that the motor torque is not under control, and the performance of the grid input side can't meet the standards of EN-61000-3-2.

Fig. 15 and Fig. 16 show the experiment results of torque control method with M = 1 and M = 5, respectively. With the *I-MR* controller is applied, the motor torque and current is under control. Meanwhile, the gain of the controller is designed to achieve a favorable inverter output torque response, and input current response as same as the simulation results. As listed in Table 2, the input power factor is high, and the input current harmonics can satisfy the recommendations of guideline EN- 61000-3-2, as shown in Fig.18.

Fig. 17 shows the experimental results of torque control loop with voltage compensation strategy. In Fig. 17(a) and Fig. 17(b), the compensation method improves the motor torque and q-axis current response. The *d*-axis feedback current fluctuation also decreases, which ensures the input current to be sinusoidal. It also improves input power factor, as listed in Table 2. In experiment, the voltage compensation strategy also reduces the input current harmonics, which is less than the values recommended in EN-61000-3-2, as shown in Fig. 18.

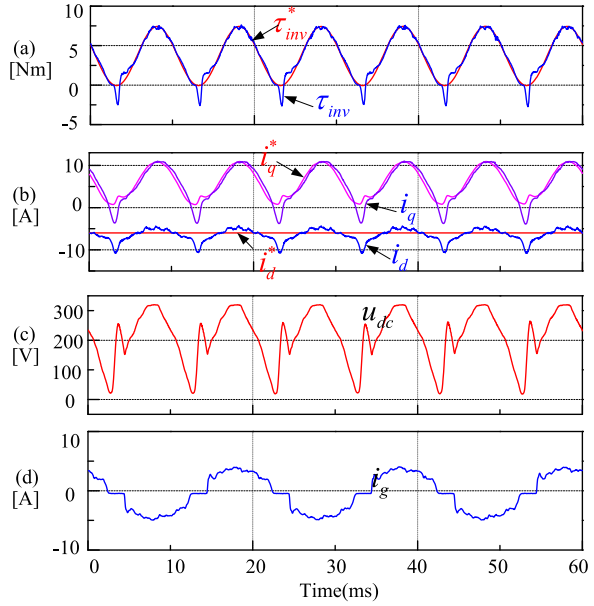

FIGURE 15. Experiment results of torque control method with M = 1. (a) The motor torque and reference; (b) the dq-axis current and references; (c) dc-link voltage; (d) grid input current.

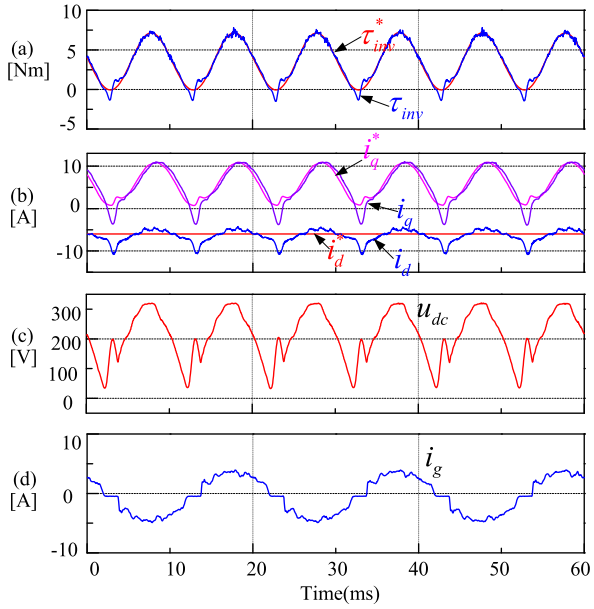

FIGURE 16. Experiment results of torque control method with M = 5. (a) The motor torque and reference; (b) the dq-axis current and references; (c) dc-link voltage; (d) grid input current.

Table 2 summarizes the input power factor and THD of grid current. It can be seen that the proposed motor torque control method has achieved effective results in both simulation and experiment. As the control delay time is not considered, the difference of simulation results is very small with different control strategies. According to Fig. 18, the voltage compensation can reduce the low-order harmonics effectively, but the high-order harmonics increased. So that so the improvement of power factor and THD is not obvious. Although the

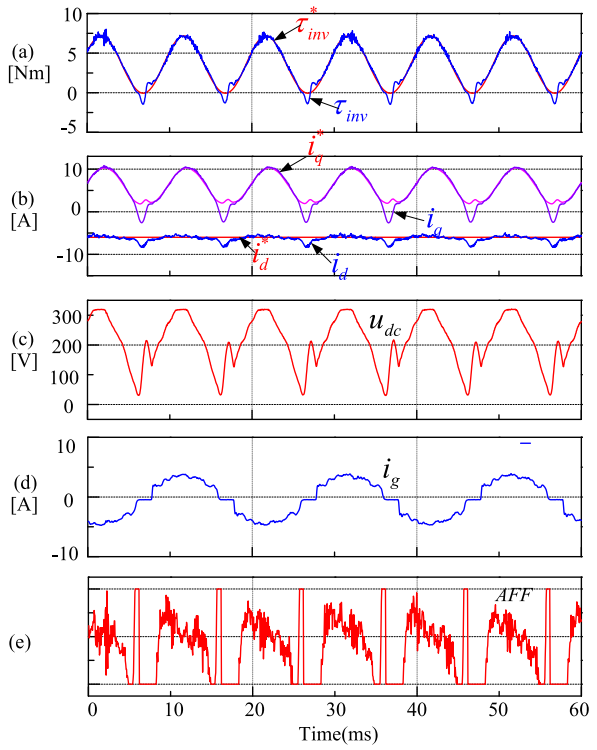

FIGURE 17. Experiment results of torque control method with voltage compensation. (a) The motor torque and reference; (b) the dq-axis current and references; (c) dc-link voltage; (d) grid input current; (e) voltage compensation gain AFF.

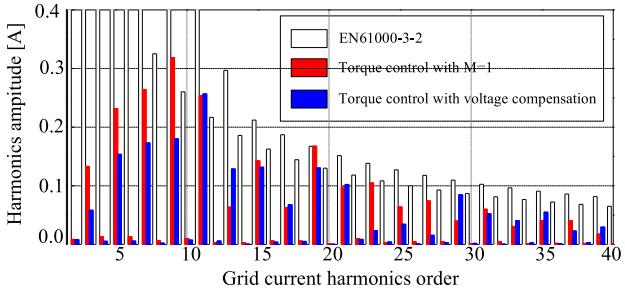

FIGURE 18. FFT analysis results of grid input current in experiment.

TABLE 2. Input power factor and the THD comparision.

	Simulation		Experiment	
	THD	Power factor	THD	Power factor
Without any control method	44.53%	91.35%	45.95%	89.11%
torque control with M=1	10.59%	99.44%	15.51%	98.82%
torque control with M=5	10.51%	99.47%	13.49%	99.10%
The proposed control method	10.24%	99.41%	12.85%	99.18%

results of simulations and experiments are slightly different, all achieve the expected control requirements.

Finally, according to Fig. 14, Fig. 18 and Table 2, the THD of the input currents is improved from 45.95% to 12.85%

by using the motor torque control method with voltage feed-forward compensation strategy. The power factor is also improved from 89.11% to 99.18%, and the grid input current harmonics are effectively reduced, that meet the standard of EN-61000-3-2.

VII. CONCLUSION

This paper proposed a motor torque control method based on integration multi-resonant controller for IPMSM drive system with small dc-link capacitor. The motor torque control loop increases the grid input power factor based on the relationship between grid input power and motor torque. However, the control performance does not follow the expectation due to the control bandwidth limitation and torque control error especially when dc-link voltage drops near zero. To deal with it, the proposed voltage feed-forward compensation can improve the inverter toque and motor current response. Results show that the power factor is up to 99.18% and the grid input current harmonics meet the regulation of EN-61000-3-2. The effectiveness of the proposed method is both verified by simulation and experiments. Nevertheless, for grid input performance is limited by the bandwidth of the current control loop, future works about expanding the bandwidth and allocating optimum dq-axis currents at the voltage saturation region are worth studying.

REFERENCES

[1] R. Dutta and M. F. Rahman, "Design and analysis of an interior permanent magnet (IPM) machine with very wide constant power operation range," *IEEE Trans. Energy Convers.*, vol. 23, no. 1, pp. 25–33, Mar. 2008.

[2] S.-Y. Jung, C. Mi, and K. Nam, "Torque control of IPMSM in the field weakening region with improved DC-link voltage utilization," *IEEE Trans. Ind. Electron.*, vol. 62, no. 6, pp. 3380–3387, Jun. 2015.

[3] F. Tinazzi and M. Zigliotto, "Torque estimation in high-efficency IPM synchronous motor drives," *IEEE Trans. Energy Convers.*, vol. 30, no. 3, pp. 983–990, Sep. 2015.

[4] H. Lamsahel and P. Mutschler, "Permanent magnet drives with reduced DC-link capacitor for home appliances," in *Proc. 35th Annu. Conf. IEEE Ind. Electron.*, Nov. 2009, pp. 725–730.

[5] M. A. Vogelsberger, T. Wiesinger, and H. Ertl, "Life-cycle monitoring and voltage-managing unit for DC-link electrolytic capacitors in PWM converters," *IEEE Trans. Power Electron.*, vol. 26, no. 2, pp. 493–503, Feb. 2011.

[6] K.-W. Lee, M. Kim, J. Yoon, S. Bin Lee, and J.-Y. Yoo, "Condition monitoring of DC-link electrolytic capacitors in adjustable-speed drives," *IEEE Trans. Ind. Appl.*, vol. 44, no. 5, pp. 1606–1613, Sep. 2008.

[7] M. Hinkkanen and J. Luomi, "Induction motor drives equipped with diode rectifier and small DC-link capacitance," *IEEE Trans. Ind. Electron.*, vol. 55, no. 1, pp. 312–320, Jan. 2008.

[8] H. Luo, K. Chen, G. Wu, and Q. Yin, "Sensorless vector control of IPMSM drive system with small DC-link capacitor," in *Proc. IEEE 10th Conf. Ind. Electron. Appl. (ICIEA)*, Auckland, New Zealand, Jun. 2015, pp. 1–6.

[9] Y. Son and J.-I. Ha, "Direct power control of a three-phase inverter for grid input current shaping of a single-phase diode rectifier with a small DC-link capacitor," *IEEE Trans. Power Electron.*, vol. 30, no. 7, pp. 3794–3803, Jul. 2015.

[10] Y. Son and J.-I. Ha, "Discontinuous grid current control of motor drive system with single-phase diode rectifier and small DC-link capacitor," *IEEE Trans. Power Electron.*, vol. 32, no. 2, pp. 1324–1334, Feb. 2017.

[11] H. Shin, Y. Son, and J.-I. Ha, "Grid current shaping method with DC-link shunt compensator for three-phase diode rectifier-fed motor drive system," *IEEE Trans. Power Electron.*, vol. 32, no. 2, pp. 1279–1288, Feb. 2017.

[12] H. Shin, Y.-H. Chae, Y. Son, and J.-I. Ha, "Single-phase grid-connected motor drive system with DC-link shunt compensator and small DC-link capacitor," *IEEE Trans. Power Electron.*, vol. 32, no. 2, pp. 1268–1278, Feb. 2017.

[13] W.-J. Lee, Y. Son, and J.-I. Ha, "Single-phase active power filtering method using Diode-Rectifier-Fed motor drive," *IEEE Trans. Ind. Appl.*, vol. 51, no. 3, pp. 2227–2236, May 2015.

[14] Y. Zhou, W. Huang, and F. Hong, "Single-phase input variable-speed AC motor system based on an electrolytic capacitor-less single-stage boost three-phase inverter," *IEEE Trans. Power Electron.*, vol. 31, no. 10, pp. 7043–7052, Oct. 2016.

[15] Y.-C. Li and C.-L. Chen, "A novel single-stage High-Power-Factor AC-to-DC LED driving circuit with leakage inductance energy recycling," *IEEE Trans. Ind. Electron.*, vol. 59, no. 2, pp. 793–802, Feb. 2012.

[16] H.-S. Jung, S.-J. Chee, S.-K. Sul, Y.-J. Park, H.-S. Park, and W.-K. Kim, "Control of three-phase inverter for AC motor drive with small DC-link capacitor fed by single-phase AC source," *IEEE Trans. Ind. Appl.*, vol. 50, no. 2, pp. 1074–1081, Mar. 2014.

[17] K. Inazuma, H. Utsugi, K. Ohishi, and H. Haga, "High-Power-Factor single-phase diode rectifier driven by repetitively controlled IPM motor," *IEEE Trans. Ind. Electron.*, vol. 60, no. 10, pp. 4427–4437, Oct. 2013.

[18] N. Zhao, G. Wang, D. Xu, L. Zhu, G. Zhang, and J. Huo, "Inverter power control based on DC-link voltage regulation for IPMSM drives without electrolytic capacitors," *IEEE Trans. Power Electron.*, vol. 33, no. 1, pp. 558–571, Jan. 2018.

[19] D. Bao, X. Pan, and Y. Wang, "A novel hybrid control method for Single-Phase-Input variable frequency speed control system with a small DC-link capacitor," *IEEE Trans. Power Electron.*, vol. 34, no. 9, pp. 9016–9032, Sep. 2019.

[20] B. Kwak, J.-H. Um, and J.-K. Seok, "Direct active and reactive power control of three-phase inverter for AC motor drives with small DC-link capacitors fed by single-phase diode rectifier," *IEEE Trans. Ind. Appl.*, vol. 55, no. 4, pp. 3842–3850, Jul. 2019.

[21] K. Abe, H. Haga, K. Ohishi, and Y. Yokokura, "Fine current harmonics reduction method for electrolytic capacitor-less and inductor-less inverter based on motor torque control and fast voltage feedforward control for IPMSM," *IEEE Trans. Ind. Electron.*, vol. 64, no. 2, pp. 1071–1080, Feb. 2017.

[22] K. Abe, H. Haga, K. Ohishi, and Y. Yokokura, "Direct DC-link current control considering voltage saturation for realization of sinusoidal source current waveform without passive components for IPMSM drives," *IEEE Trans. Ind. Electron.*, vol. 65, no. 5, pp. 3805–3814, May 2018.

[23] H. Li, K. Huang, H. Luo, and Q. Yin, "A motor torque control method based on integration quasi-resonant controller for reduced DC-link capacitance IPMSM drive system," in *Proc. 14th IEEE Conf. Ind. Electron. Appl. (ICIEA)*, Xi'an, China, Jun. 2019, pp. 1290–1295.

[24] M. Ciobotaru, R. Teodorescu, and F. Blaabjerg, "A new single-phase PLL structure based on second order generalized integrator," in *Proc. 37th IEEE Power Electron. Specialists Conf.*, Jun. 2006, pp. 1–6.

[25] A. Kuperman, "Proportional-resonant current controllers design based on desired transient performance," *IEEE Trans. Power Electron.*, vol. 30, no. 10, pp. 5341–5345, Oct. 2015.

[26] Y. Basha, A. Belenky, and A. Kuperman, "Tracking performance oriented design of proportional-resonant controllers under finite control bandwidth and actuator delay," in *Proc. IEEE Int. Conf. Sci. Electr. Eng. (ICSEE)*, Nov. 2016, pp. 1–5.

[27] L. B. G. Campanhol, S. A. O. da Silva, A. A. de Oliveira, and V. D. Bacon, "Dynamic performance improvement of a grid-tied PV system using a feed-forward control loop acting on the NPC inverter currents," *IEEE Trans. Ind. Electron.*, vol. 64, no. 3, pp. 2092–2101, Mar. 2017.

[28] B. L. G. Costa, V. D. Bacon, S. A. O. da Silva, and B. A. Angelico, "Tuning of a PI-MR controller based on differential evolution Metaheuristic applied to the current control loop of a shunt-APF," *IEEE Trans. Ind. Electron.*, vol. 64, no. 6, pp. 4751–4761, Jun. 2017.

[29] T. Ye, N. Dai, and C. Lam, "Wong, M.; Guerrero, J. M. Analysis design and implementation of a quasi-proportional-resonant controller for multi-functional capacitive-coupling grid-connected inverter," *IEEE Trans. Ind. Appl.*, vol. 52, no. 5, pp. 4269–4280, Sep/Oct., 2016.

[30] W. L. Soong and N. Ertugrul, "Field-weakening performance of interior permanent-magnet motors," *IEEE Trans. Ind. Appl.*, vol. 38, no. 5, pp. 1251–1258, Sep. 2002.

[31] S. Morimoto, Y. Takeda, T. Hirasa, and K. Taniguchi, "Expansion of operating limits for permanent magnet motor by current vector control considering inverter capacity," *IEEE Trans. Ind. Appl.*, vol. 26, no. 5, pp. 866–871, 1990.

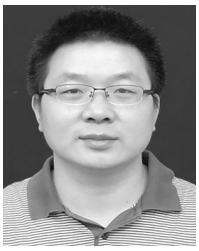

HAICHUN LI received the B.S. and M.S. degrees from the School of Automation, Huazhong University of Science and Technology, Wuhan, China, in 2006 and 2008, respectively. He is currently pursuing the Ph.D. degree in power electronics and electrical drives with the School of Artificial Intelligence and Automation, Huazhong University of Science and Technology.

His current research interests include intelligent control of permanent magnet synchronous motor drives and high-performance servo systems.

QUAN YIN received the B.S. and M.S. degrees in industrial electrical automation and the Ph.D. degree in control theory and control engineering from the Huazhong University of Science and Technology, Wuhan, China, in 1990, 1995, and 2001, respectively.

He was a Postdoctoral Fellow with the Huazhong University of Science and Technology, from 2001 to 2003, where he is currently a Professor with the School of Artificial Intelligence and Automation. His current research interests include intelligent control and embedded control systems.

QINGYI WANG received the B.S. degree in industrial electrical automation and the M.S. and Ph.D. degrees in control theory and control engineering from the Huazhong University of Science and Technology, Wuhan, China, in 1996, 2004, and 2008, respectively.

He is currently an Associate Professor with the School of Automation, China University of Geosciences. His current research interests include renewable energy systems, power electronics, and control in energy systems.

JIGUI MIAO received the B.S. degree from the School of Electronic Engineering, Xi'an Shiyou University, Xi'an, China, in 2018. She is currently pursuing the M.S. degree in power electronics and electrical drives with the School of Artificial Intelligence and Automation, Huazhong University of Science and Technology, Wuhan, China.

Her current research interests include intelligent control and application of machine learning in power electronics and motor drive.

YANTING HOU received the B.S. degree from the Faculty of Automation and Information Engineering, Xi'an University of Technology, Xi'an, China, in 2010.

She is currently an Engineer with Guangdong Elesy Electric Company, Ltd., Foshan, China. Her current research interests include intelligent control and application of permanent magnet synchronous motor drives and high-performance servo systems.